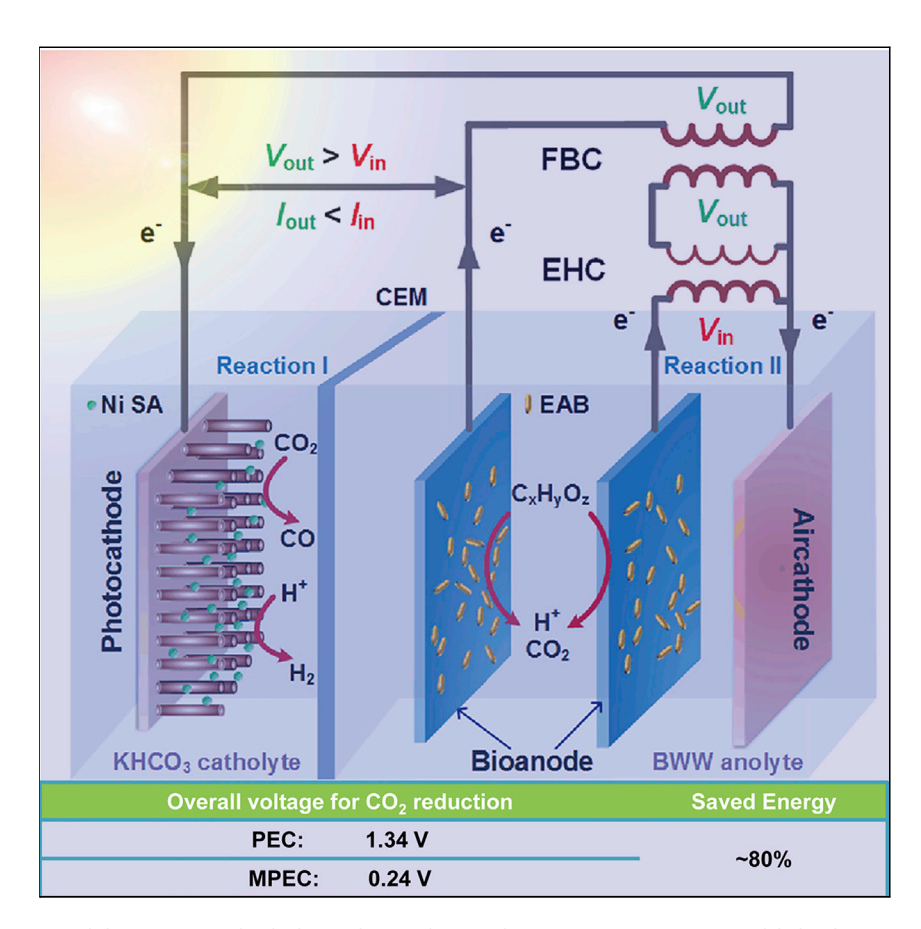




Article

Spontaneous Solar Syngas Production from CO₂ Driven by Energetically Favorable Wastewater Microbial Anodes



An elaborate microbial photoelectrochemical (MPEC) system was established to produce syngas without any external energy input. In this setup, the microbial anode is capable of oxidizing waste organics in wastewater and reducing $\rm CO_2$ on the photocathode. The Si photocathode coated with Ni single-atom catalysts was powered by the microbial anode and delivered a flexibly tunable syngas production.

Lu Lu, Zhida Li, Xi Chen, ..., Xiaoqing Pan, Zhiyong Jason Ren, Jing Gu

zjren@princeton.edu (Z.J.R.) jgu@sdsu.edu (J.G.)

HIGHLIGHTS

A microbial photoelectrochemical system achieved unassisted CO₂ reduction

Energy is recovered from both wastewater and sunlight to conquer CO₂ reduction

The CO:H₂ ratio could be flexibly tuned from 0.1 to 6.8

Water-energy-carbon problems were synergistically solved in one system

Lu et al., Joule 4, 1–13 October 14, 2020 © 2020 Elsevier Inc. https://doi.org/10.1016/j.joule.2020.08.014

Joule



Article

Spontaneous Solar Syngas Production from CO₂ Driven by Energetically Favorable Wastewater Microbial Anodes

Lu Lu,^{1,2,6} Zhida Li,^{3,6} Xi Chen,² Huan Wang,² Sheng Dai,⁴ Xiaoqing Pan,^{4,5} Zhiyong Jason Ren,^{2,*} and Jing Gu^{3,7,*}

SUMMARY

The photoelectrochemical (PEC) reduction of CO₂ to syngas is an attractive strategy for solar-to-fuel conversion. However, the high overpotential, inadequate selectivity, and high cost demand for alternative solutions. Here, we demonstrate a hybrid microbial photoelectrochemical (MPEC) system that contains a microbial anode capable of oxidizing waste organics in wastewater and reducing the oxidation potential by 1.1 V compared with abiotic water oxidation using a PEC anode. Moreover, the MPEC employs a power management circuit (PMC) to enable parallel low-energy-producing reactions operated in the same solution medium to conquer highoverpotential reactions. The nanowire silicon photocathode integrated with a selective single-atom nickel catalyst (Si NW/Ni SA) achieved up to ~80% faradic efficiency for CO generation with a highly tunable CO:H₂ generation ratio (0.1 to 6.8). When the bioanode was coupled with the Si NW/Ni SA, up to 1.1 mA cm⁻² of spontaneous photocurrent density was obtained for high-rate syngas generation.

INTRODUCTION

Solar-driven CO₂ conversion to fuels and chemicals offers a sustainable pathway for renewable energy storage and CO₂ valorization. Artificial photosynthesis (APS) emulates natural photosynthesis and carries great promise due to its high efficiency and product flexibility.^{2,3} Similar to natural photosynthesis, APS systems use water as electron and proton sources for fixing CO₂. However, unlike natural photosynthesis, APS systems utilize semiconductor materials to absorb light and catalysts to facilitate kinetics of chemical conversions. CO₂ reduction reaction (CO₂RR) is an energy-intensive process. For example, reduction of CO₂ to CO requires a minimum thermodynamic voltage of 1.34 V (Figure 1A and details in Supplemental Information), 4 while in reality, an additional $\sim 1 \text{ V}$ is usually required to overcome the high activation-barrier-induced overpotential losses, making the overall energy consumption higher than 2 V.5 Most semiconductors either suffer from limited photovoltage or unsuitable band edge positions to conquer the thermodynamic and kinetic challenges of CO₂RR. Thus, solar-driven CO₂RR typically requires additional energy input.⁶ Figure 1A demonstrates commonly used semiconductors' band edge and redox potentials for CO₂ reduction and H₂O oxidation, and it can be seen that only a few semiconductors' band edge positions can straddle the redox potentials of CO₂ reduction and H₂O oxidation. To overcome this energetic deficiency, previous studies had to provide an extra bias either by connecting multiple photovoltaics in series to drive an electrolyzer (PV-electrolyzer)^{4,6} or by employing a complex

Context & Scale

Converting CO₂ into value-added chemicals holds good promise for carbon valorization, but current methods rely heavily on electricity. In the same context, wastewater as another abundant waste carbon source also requires significant energy inputs to clean. Thus, exploring alternative scientific approaches to synergistically address water, energy, and carbon challenges becomes an emerging need. This study reported a microbial photoelectrochemical (MPEC) system consisting of electroactive microbial bioanodes and a Sinanowire photocathode coated with Ni single-atom catalysts. The photocathode and bioanodes converted solar energy and chemical energy of waste organics in wastewater, respectively, into electrical energy, which enabled uphill reactions to overcome the thermodynamic barriers in CO₂ reduction to generate syngas with tunable CO:H2 ratios via a power management circuit (PMC). This new hybrid approach presents a new pathway to tackle carbon, water, and energy challenges together.





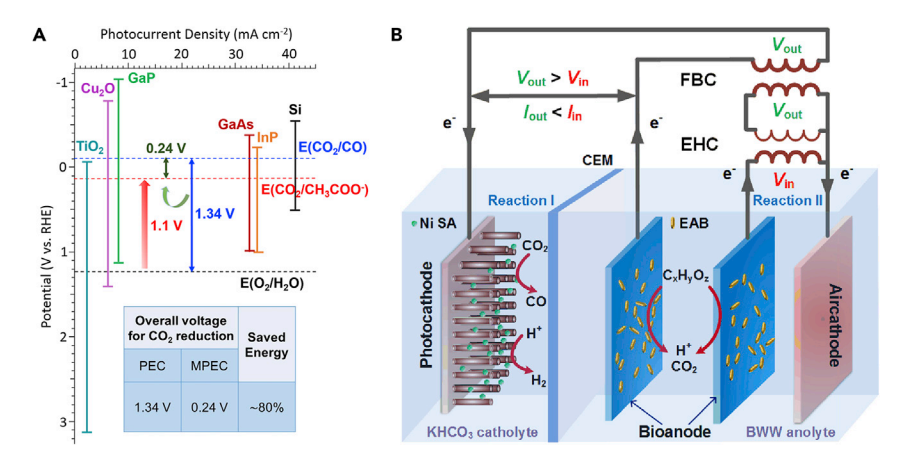


Figure 1. Schematic of Band Positions of Common Semiconductors and an Energetically Favorable Microbial Photoelectrochemical (MPEC) System Involved in the Spontaneous Solar CO₂ Reduction to Syngas

(A) Conduction (upper bar) and valence band (lower bar) positions versus RHE of potential semiconductors used for photoelectrochemical CO_2 reduction under 1 sun condition (100 mW/cm²). The thermodynamic potentials for CO_2 reduction to CO, water oxidation, and acetate (organic) oxidation are indicated by blue, black, and red dotted lines, respectively. (B) Proposed MPEC system for spontaneous solar-driven CO_2RR . The voltage (V_{in}) generated by coupling waste organics $(C_XH_YO_2)$ oxidation on one electroactive bioanode with oxygen reduction on an air cathode (Reaction II) was first boosted to a larger output voltage (V_{out}) by an energy-harvesting circuit (EHC). The electrical energy produced was temporarily stored as electromagnetic energy. Further, a flyback circuit (FBC) was able to isolate V_{out} from Reaction II to power the solar-driven CO_2RR on a photocathode, which is coupled with another electroactive bioanode (Reaction I). The FBC decouples Reactions I and II and combines them in one solution environment without inducing a chemical short-circuit. The waste organics $(C_XH_YO_Z)$ in brewery wastewater (BWW) served as electron donors.

multijunction tandem photoelectrode. 7,8 Among the different products ranging from alcohols and olefins to organic acids converting from CO_2 , 1,2 tunable syngas (a mixture of CO and H_2) has been a popular target, as it is a common and robust chemical feedstock, which can be upgraded easily to a variety of multicarbon fuels and commodity chemicals via Fischer-Tropsch (FT) synthesis or biocatalytic fermentation. 9,10

The unbiased APS systems currently face major barriers of complex fabrication, limited device lifetime, and low stability and scalability. 2,6 In this context, recent development on microbial electrochemistry and electrical circuitry provide unprecedented opportunities to overcome the aforementioned challenges. 11,12 For example, microbial photoelectrochemical (MPEC) systems couple photocathodes with microbial anodes, where microbial electrochemical oxidation (MEO) was used to replace water oxidation reaction (OER) in conventional APS systems. 13-15 Recent studies have demonstrated that the bioanode can significantly reduce the overall energy requirement of a redox reaction, such as hydrogen (H₂) evolution reaction, by more than 1 V. 14,16 Up to 23 mA /cm² self-sustaining photocurrent density could be achieved when a Si photocathode was coupled with microbial bioanodes for concurrent H₂ production and brewery wastewater treatment. ¹⁶ However, to the best of our knowledge, no previous work has reported a spontaneous CO2-reduction MPEC system, because CO₂RR is a much more challenging reaction than H₂ evolution and requires much higher compensation on overpotential. The MPEC bioanode uses indigenous electroactive bacteria to oxidize any biodegradable compounds¹⁷ (e.g., carbohydrates, proteins, cellulose, organic acids, hydrocarbons, etc.) in

https://doi.org/10.1016/j.joule.2020.08.014

¹School of Civil and Environmental Engineering, Harbin Institute of Technology, Shenzhen 518055, China

²Department of Civil and Environmental Engineering and Andlinger Center for Energy and the Environment, Princeton University, Princeton, NJ 08544, USA

³Department of Chemistry and Biochemistry, San Diego State University, 5500 Campanile Drive, San Diego, CA 92182, USA

⁴Department of Materials Science and Engineering, University of California Irvine, Irvine, CA 92697, USA

⁵Department of Physics and Astronomy, University of California Irvine, Irvine, CA 92697,

⁶These authors contributed equally

⁷Lead Contact

^{*}Correspondence: zjren@princeton.edu (Z.J.R.), jgu@sdsu.edu (J.G.)





wastewater to recover and convert energy imbedded in waste organics as electricity. Further, the recovered electricity is supplied to the photocathode, reducing the overall redox-reaction energetic requirements (Figures 1A and 1B). Considering the common wastewater constituent acetate as an example, 11 the theoretical energy required for $\rm CO_2RR$ when coupled with water oxidation is 1.34 V; however, integrating MEO with $\rm CO_2RR$ leads to a significantly reduced overall voltage (0.24 V), leading to $\sim\!80\%$ less energy need than that of an photoelectrochemical (PEC)-based APS system (Figure 1A and more details in Supplemental Information). This is a superior strategy compared with the direct addition of sacrificial reagents 18 to reduce the overall potential of an electrochemical system, as wastewater is essentially free and microbial anodes are extremely stable. 18,19 Besides, the microbial electrochemical system has been scaled up to pilot scales using actual wastewater streams, generating additional environmental benefits. 20

Theoretically, CO₂RR can be driven spontaneously by coupling a bioanode with a photocathode because the conduction and valence band edges of most semiconductors straddle the CO₂ reduction and MEO potentials (Figure 1A).⁶ However, because CO₂RR has a much higher activation barrier (or overpotential) than H₂ evolution, a simple coupling of a photocathode with a bioanode cannot overcome the kinetic barriers. Here, we employed a tailorable power management circuit (PMC) capable of capturing and storing energy from microbial reactions to overcome the energy barriers for the uphill CO₂RR. ^{18,21} Specifically, we coupled the electroactive microbial anode with a low-cost silicon (Si) nanowire (Si NW) photocathode coated with Ni single-atom catalysts (Ni SA) for PEC CO₂RR (Reaction I, 0.24 V required) (Figure 1B). The nanowire Si interface possesses a dramatically increased surface area relative to planar Si, thus enhancing light-absorbing properties and activity.²² To lower the overall activation barrier of the reaction, a highly active and cost-effective single-atom Ni catalyst^{23,24} was developed and coated onto Si NW dropwise to form a Si NW/Ni SA interface. Si NW/Ni SA demonstrates superior activity toward syngas generation when converting CO_2 and H_2O simultaneously, with a highly tunable CO:H₂ generation ratio (0.1 to 6.8).

Herein, we demonstrate for the first time that an MPEC system accomplished spontaneous CO_2 reduction with tunable syngas ratios while simultaneously removing waste organics. This is a cost-effective novel solution to potentially close the carbon-emission loop by decomposing organics in wastewater for energy extraction, electron and proton release, and CO_2 conversion into profitable fuels in a self-assisted manner without any external bias.

RESULTS

Characterization of Ni Single-Atom Catalysts

Atomically dispersed Ni was supported onto nitrogen-doped carbon derived from pyrolysis of zeolitic imidazolate fromwwork-8 (ZIF-8), as in previous literature.²⁵ To reveal the surface morphology of the single-atom Ni on nitrogen-doped carbon (Ni SA/N-C), aberration-corrected scanning transmission electron microscopy (AC-STEM) combined with energy dispersive X-ray spectroscopy (EDS) was performed (Figure 2). The carbon substrate derived from ZIF-8 was annealed under nitrogen atmosphere, resulting in uniform rhombododecahedral shapes with an average size of ~100 nm (Figure 2A). The EDS elemental maps displayed in Figures 2B and 2C confirm a homogeneous Ni distribution throughout the carbon support. Particularly, as shown in the atomic-resolution high-angle annular dark field (HAADF)-STEM image (Figure 2D), the bright spots corresponding to the individual





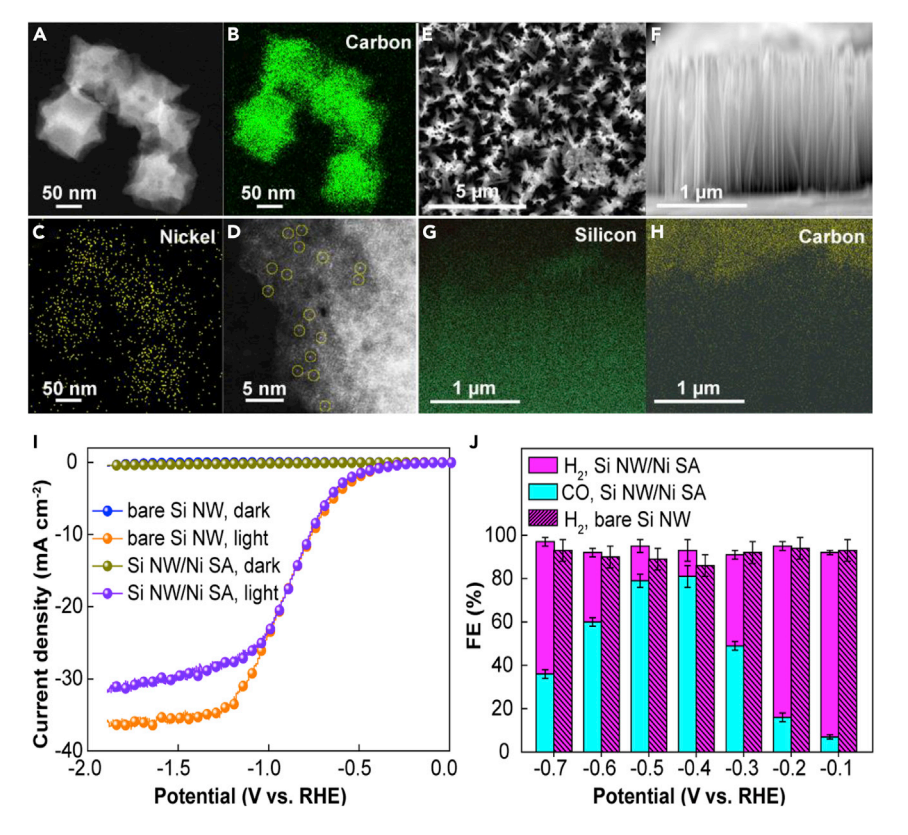


Figure 2. Characterization of the Ni SA/N-C Catalyst and Photocathodes

- (A) HAADF STEM images of NiSA/N-C.
- (B) EDS maping of carbon on NiSA/N-C.
- (C) EDS mapping of nickel on NiSA/N-C.
- (D) HAADF-STEM image of Ni SA. The yellow circles highlight a few representative Ni single atoms on the carbon surface. Characterization of the Si NW/Ni SA.
- (E) Top-view SEM.
- (F) Cross-sectional SEM.
- (G) EDS mapping of silicon.
- (H) EDS mapping of carbon. Due to the low concentration of single-atom Ni, it is difficult to identify the Ni element from EDS mapping.
- (I) Photocurrent density-potential (J-V) curves of bare Si NW and Si NW/Ni SA. LSV scans were performed at 5 mV/s in CO₂ saturated 0.25 M KHCO₃ electrolyte (pH 7) under 1 sun illumination or dark conditions.
- (J) FE of the Si NW/Ni SA and bare Si NW toward CO or $\rm H_2$ production at different potentials. Data were collected from the initial 30 min at each potential. The error bars were obtained by repeating experiments for three times at each potential.

Ni atoms could be clearly identified due to the distinguishable Z-contrast differences between Ni and carbon support. 26

The Ni SAs/N–C catalyst was further characterized by surface-sensitive X-ray photo-electron spectroscopy (XPS) (Figure S1; Supplemental Information) to elucidate its chemical composition and states. The high-resolution N 1s XPS spectrum (Figure S1A) was deconvoluted into the following components: pyridinic N (\sim 398.7 eV), N-Ni species (\sim 399.6 eV), ²⁷ pyrrolic N (\sim 400.7 eV), graphitic N (\sim 401.7 eV), and oxidic N (\sim 403 eV). The dominant pyridinic N on carbon has been well recognized previously as efficient metal-coordination sites. ²⁸ The existence of graphitic N species is further confirmed by the C=N bond shown in the C 1s spectrum





(Figure S1B). The binding energy of the Ni 2p3/2 peak is located at \sim 855 eV, which is higher than that of Ni⁰ (\sim 852.6 eV)²⁹ but lower than Ni²⁺ (\sim 857.1 eV) (Figure S1C),³⁰ indicating that the Ni species' valence state is situated between Ni⁰ and Ni²⁺. This result coincides well with the N 1s spectrum, which shows the formation of N-Ni bond and the electron transfer from Ni atom to nitrogen-doped carbon support.

The atomically dispersed Ni showed an excellent selectivity toward converting CO_2 into CO due to its low-valent configuration. ^{24,25,29} The faradic efficiency (FE) for CO production reported herein is close to 100% at -0.8 V versus RHE, as presented in Figure S2. Here, Ni SA did demonstrate its profound selectivity for CO_2RR when competing with hydrogen evolution reaction (HER) in an aqueous medium. ²⁹

Characterization of Catalytic Photoelectrodes for CO₂ Reduction

To construct an effective interface between photoelectrode and catalyst, the Ni SA/N–C catalyst was consequently drop casted onto Si NWs. Representative top-view and cross-sectional SEM images of the bare Si NW are presented in Figures S3A and S3B, respectively. After loading Ni SA/N–C, the N–C was observed to disperse uniformly across the surface of the Si NW (Figures 2E and 2F), as confirmed by the EDS mapping (Figures 2G and 2H).

To evaluate the catalytic performance of Ni SAs on the Si photoelectrode (Si NW/Ni SA), linear sweep voltammetry (LSV) was conducted (Figure 2I). The cathodic current densities under dark conditions for both bare Si NW and Si NW/Ni SA were negligible. Under 1 sun illumination, both photocathodes exhibited similar onset potentials of -0.3 V versus RHE under neutral conditions. Nevertheless, the bare Si NW showed a slightly higher light-limited current density than the Si NW/ Ni SA, possibly due to the slight light-blocking effect induced by interfacial modification or the faster kinetics of HER relative to CO₂RR.³¹ Although both Si interfaces have similar J-V curves, they represent completely different reaction processes. In the absence of the Ni SA/N-C catalyst, Si NW yielded negligible production of CO at all applied potentials (Figure 2J). Meanwhile, the FE for H₂ production approached approximately 100%, indicating that all generated charge carriers are used for converting water into H₂. In contrast, the Si NW/Ni SA demonstrated significantly enhanced selectivity toward CO production, with an optimal FE of over 80% for CO production at -0.4 V versus RHE, with up to \sim 400 mV reduced overpotential compared with non-solar-assisted Ni SA catalysts (Figure S2). The CO:H2 ratios can be tuned between 0.1 to 6.8 by simply adjusting bias from -0.1 to -0.7 V versus RHE. The expanded syngas ratio range also allows this photoelectrode to be a great candidate for producing hydrocarbons in Fischer-Tropsch processes. 10

The dependence of CO partial current density on applied potentials is shown in Figure S4A, where higher overpotential delivers a larger CO partial current density, which agrees well with previous work. The calculated turnover frequency (TOF) of SA Ni on Si (Figure S4B) reaches over 7000 h $^{-1}$ at -0.4 V versus RHE, which is comparable with or even better than the state-of-the-art single-atom catalysts for CO $_2$ RR, including Ni SA (5273 h $^{-1}$ at -1.0 V versus RHE) 25 and diatomic Ni-Fe SA (7,682 h $^{-1}$ at -1.0 V versus RHE). However, with the photo-assisted effect, the overpotential was greatly reduced by $\sim\!400$ mV. The incident photon-to-current efficiencies (IPCE) of the photocathode were measured in 0.25 M KHCO $_3$ at -1.2 V versus RHE, where the dark current was negligible (Figure S4C). The maximum efficiency was achieved at 900 nm and equal to $\sim\!46$ %, comparable to other nanostructured n $^+$ p-Si photoelectrodes. In addition, the intrinsic energy efficiencies of Si NW photocathodes alone for H $_2$ production in acidic electrolyte were 0.32% (bare





Si NW) and 3.56% (Si NW/Pt) that were tested according to previous studies ^{16,33,34} (Figure S4D, details of calculation are provided in Supplemental Information). The stability of the Si NW/Ni SA was further analyzed by long-term electrolysis (Figure S4E). The FE toward CO production decreased from the initial >80% to ~60% after a 10-h electrolysis, which may be attributed to Ni SA/N–C catalyst drifting from the top surface to the bottom along the nanowire array, which was confirmed by postelectrolysis SEM (Figure S5). The photocathode performance was further compared with other state-of-the-art photoelectrodes for syngas production (Table S1). Since a simple single-junction Si NW photocathode was employed here, the onset potential of this photocathode interface was comparable with other multijunction photocathodes, but the FE toward selective CO₂ reduction to CO distinguished this interface from other photoelectrodes, where the optimal FE of this PEC interface was 81% while others were lower than 72% (Table S1). Moreover, by easily tailoring the applied potentials, the syngas ratio (CO:H₂) could be tuned from 0.1 to 6.8, which was larger than most other PEC systems.

Power Management Circuit (PMC) Integration for Energetically Favorable Reactions

Using this MPEC system, the overall voltage required for the CO2RR (Reaction I in Figure 1B) has been greatly reduced from 1.34 to 0.24 V by coupling a Si photocathode with a wastewater bioanode. These two electrodes were conductively connected to form a closed circuit. When Si NW/Ni SA was coupled with a bioanode (Reaction I), negligible spontaneous photocurrent (10–15 μA/cm²) was generated. Therefore, another bioanode coupled with an air cathode (O2 reduction) termed as "energy production" portion (Reaction II) was added to Reaction I (Figure 1B). Reaction II generated an open circuit voltage of 1.1 V (Equation 15 in Supplemental Information), or a voltage of 0.4 V with circuit load (Figure 3D, cyan curve). Since an extra input of 0.4 V might not be the optimal bias for CO₂RR, a PMC was employed here to fine-tune Reaction II's bias output. 18,21 The PMC contained two subcircuits (Figure 1B): first, an energy-harvesting circuit (EHC) that utilizes a pulse-frequency modulation boost-converter and charger to first boost the output voltage (0.4 V) derived from reaction II to a higher voltage of 0.7 V (Figure 3C, cyan curve). Second, a flyback circuit (FBC), a transformer-based direct current (DC)-DC converter, was used to electrically isolate Reaction I from Reaction II under the control of a tailored oscillator and timer. Here, the extra PMC played central roles to boost and fine-tune the voltage of the Reaction II, isolating the generated currents. DC isolation allowed the energy transfer between two circuits for Reactions I and II. However, the two circuits did not need to be electrically connected as in a conventional circuit. Each circuit maintained its own current loop with independent current generation (Figures 3A and 3B). This enabled two different reactions to share the same electrical ground and co-exist in the same analyte, which generally leads to a chemical short circuit without the manual DC isolation. 18,21 Such a strategy allows energy production from several simple reactions to work together and realize an uphill overall reaction in the same solution medium otherwise thermodynamically and kinetically unfavorable. In previous PEC systems, it was considered impossible to fine-tune the bias on photovoltaic junctions. For this specific reaction, the boosted bias can be tailored by modifying parameters in the energy-harvesting circuit (Reaction II), which allowed a fine-tuned photocathode potential resulting in identification of optimal product ratios (Figure 2J). In this MPEC system, a fine-tuned prototype -0.4 to -0.5 V versus RHE potential was supplied by Reaction II to the photocathode to maintain a maximum CO:H₂ production ratio, correlating with the photocathode performance shown in Figure 2J.



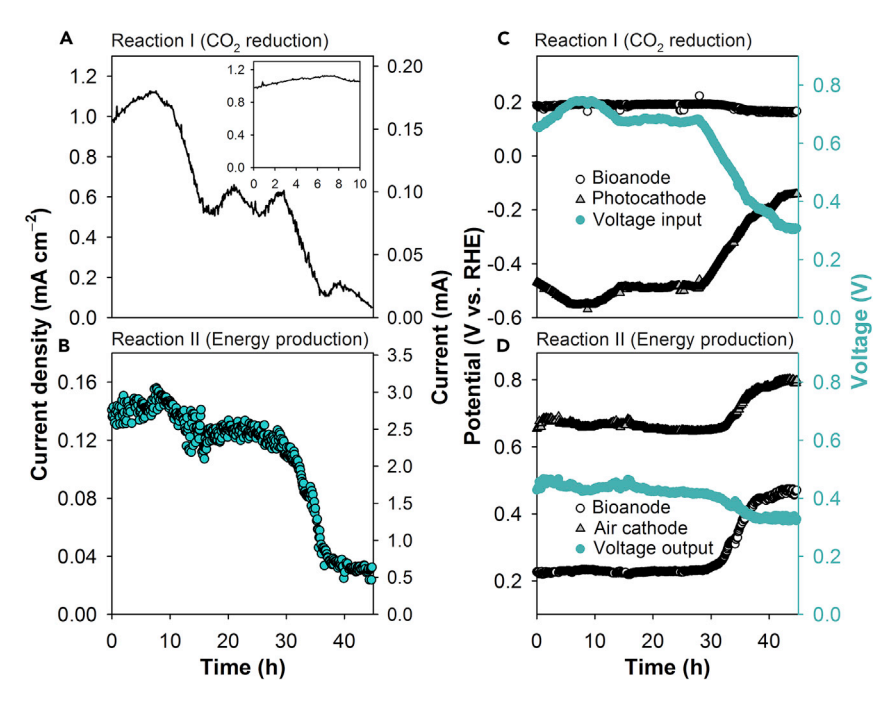


Figure 3. Current Generation and Electrode Potentials in MPEC during a Fed-Batch Cycle

- (A) Photocurrent generation for solar-assisted CO2 reduction in Reaction I. Inset (A) is the photocurrent density generated during the first 10 h. Current densities were calculated based on the projected area of photocathode (Reaction I).
- (B) Current generation in Reaction II. Current densities were calculated based on the projected area of aircathode (Reaction II).
- (C) Electrode potentials and voltage input for solar assisted CO2 reduction in Reaction I. The voltage input was provided by Reaction II and was boosted and isolated by energy-harvesting and flyback circuits, respectively.
- (D) Electrode potentials and voltage output in Reaction II.

Photocurrent Generation for CO₂RR in the Integrated MPEC System

A maximum photocurrent density of 1.0-1.1 mA cm⁻² (0.16-0.18 mA) could be constantly generated for CO₂RR during the first 10 h in each fed-batch cycle (Figures 3A and S6). This correlated well with the stable performance of the photocathode over 10 h of electrolysis (Figure S4E). The photocurrent decreased within the consequent 6 h, reaching a plateau of 0.5-0.7 mA cm⁻² during 16-29 h. The decreased photocurrent was mainly attributed to the performance decay of the photocathode rather than the coupled bioanode or the energy harvest circuit. Because the bioanode potential (-0.2 V versus RHE) and the voltage input remained stable (~ 0.7 V) during the whole 29 h (Figure 3C), the supplied waste organics (electron donors) utilized by both Reactions I and II were sufficient. Moreover, numerous previous studies have shown that a bioanode can be kept stable over several years once the microbial conversion process was established with sufficient organic substrates. 11,16 After 29 h, the depletion of organics in the analyte led to a sharp decrease of current and power output in Reaction II (Figure 3B), reflected by the reduced bias applied to Reaction I (Figure 3C) and a decrease in photocurrent density for CO₂ reduction (Figure 4A). During the period of stable voltage output, the current generation in Reaction II was 2.2-3.1 mA (0.11-0.16 mA cm⁻²), which was an order of magnitude higher than the photocurrent produced solely from Reaction I. The corresponding power-conversion efficiency between Reaction I and II was determined to be ~11.4 %, indicating that only one-tenth of the energy produced by Reaction II was used to for spontaneous CO2 conversion, with the remaining



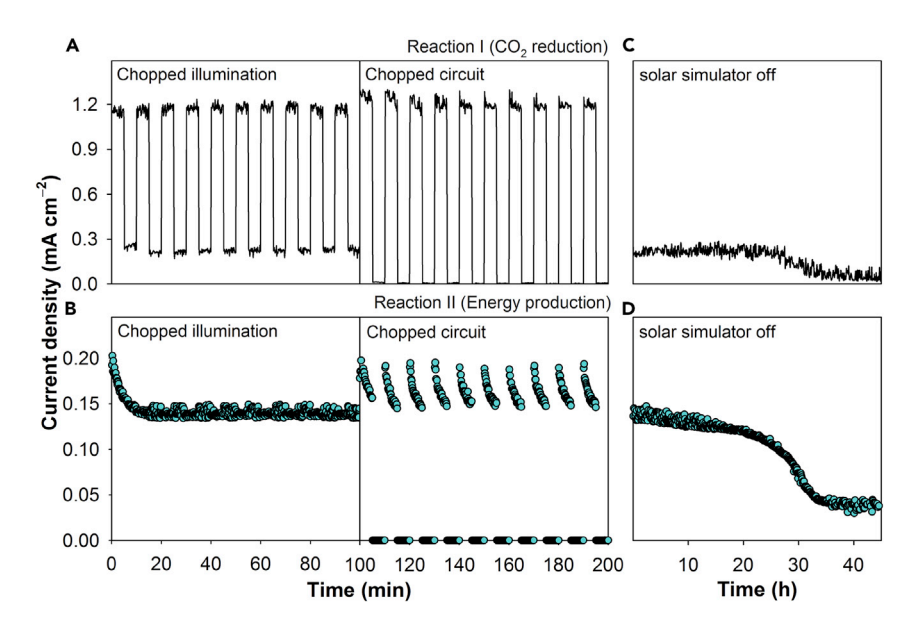


Figure 4. Current Density-Time (J-t) Curves under On and Off Solar Illumination and Connection and Disconnection of the Energy-Production Circuit (Reaction II) in MPEC (A) Current densities of Reaction I under chopped illumination and circuit.

- (B) Current densities of Reaction II under chopped illumination and circuit.
- (C) Current densities of Reactions I with the solar simulator switched off during a fed-batch cycle. Current densities were calculated based on the projected area of photocathode (Reaction I).
- (D) Current densities of Reactions II with the solar simulator switched off during a fed-batch cycle. Current densities were calculated based on the projected area of air cathode (Reaction II).

amount being consumed by the PMC. Further optimizations could improve the overall energy efficiency by reducing the PMC energy loss. 12

Photocurrent generation in Reaction I was triggered instantaneously by solar irradiation (Figure 4A). Light had no influence on current generation in the energy-harvesting circuit (Reaction II) (Figure 4B). Interestingly, a small photocurrent density of ~ 0.3 mA cm⁻² was detected after the solar simulator was switched off. This photocurrent generation was likely due to the room-light irradiation, as it became negligible after placing the reactor to a dark room (Figure S8). Moreover, we found that the bias produced by Reaction II was critical for the generation of all photocurrent, as it instantaneously declined to 10–15 μA/cm² even under illumination conditions once the Reaction II circuit was disconnected. This observation was further supported by the low current generation without the solar simulator during 30 h of electrolysis. Before organic-waste depletion (indicated by current generation in Reaction II, Figure 4D), up to 0.3 mA cm⁻² current was generated from Reaction I. After depletion of organic waste, current dropped to a negligible level due to the lack of bias produced by Reaction II at the end of a fed-batch cycle (Figures 4C, 4D, and 3C). The two bioanodes in MPEC removed a total of 91% \pm 2% waste organics, which were converted into current in Reaction I and II with a total Coulombic efficiency of 17% \pm 0% (Figure S9). The rest of removed organics that were not converted to current were generally oxidized by abundant nonelectroactive bacteria native to real wastewater or were used to synthesize microbial cells on the bioanode.

Syngas Production

The CO:H₂ ratio was affected by both the photocathode properties and electrical potential. The photocathode potential was stable during the 29-h test and ranged





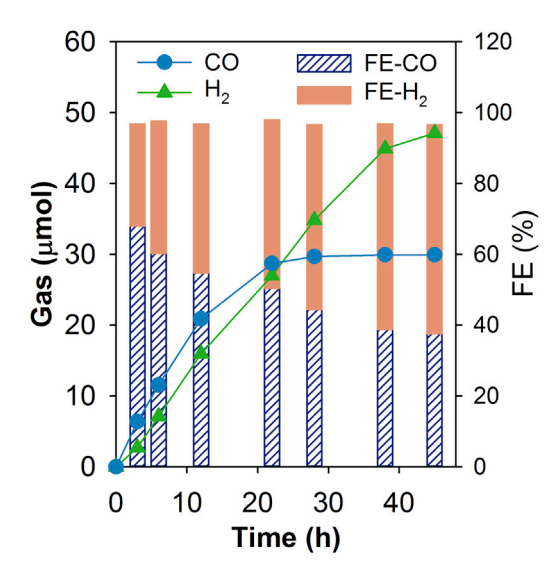


Figure 5. Syngas Production in MPEC

Amount and FE of accumulative CO and H_2 production with the time during a fed-batch cycle.

between -0.46 and -0.57 V versus RHE (Figure 3C), at which the FE for CO was 60%-80% (Figure 2J). However, the CO selectivity at each potential decreased over time due to changes of the Si NW/Ni SA interface. In MPEC, the FE of accumulative CO was 60%-68% for the first 6 h with a CO:H2 ratio of 1.6-2.3 and a total FE (CO and H₂) ranging from 96.8% to 97.6% (Figure 5). After that, the FE toward CO further decreased to 55% (12 h) and 50% (22 h), respectively, consistent with the half-cell photocathode testing (Figure S4E). Almost all photocurrents were further employed for H_2 evolution after 30 h, leading to a total CO: H_2 ratio of 0.6 at the end of batch cycle (45 h). The total FE of CO and H₂ during an entire process was higher than 96.6%, indicating profound selectivity of this system toward syngas production. The syngas with CO:H₂ ratios between 0.5 and 1 are ideal for manufacturing methanol³⁵ and dimethyl ether.³⁶ During a batch cycle, the energy efficiency of the complete process was quantified by 0.43%-0.67%, which was calculated by a ratio of energy contained in the chemical products (H₂ and CO) over the total energy input, including both incoming light energy and chemical energy added by the substrate (details of the calculation are provided in the Supplemental Information).

DISCUSSION

Due to CO₂RR's high activation barrier, to date few PEC works can achieve nonbiased CO₂RR (Table S2). For conventional self-sustaining PEC (or photovoltaic) systems, at least 2.1 V of cell voltage is necessary in order to generate a recognizable photocurrent toward CO₂RR. For the first time, MPEC employed waste organics in wastewater as electron and proton sources to significantly reduce the bias to only one-third of that needed in previous PEC systems (Table S2). This setup presented tremendous improvement in terms of energetics by replacing abiotic anodes (water oxidation) with wastewater bioanodes (waste organics oxidation). Moreover, a PMC was employed to decouple the two chemical reactions in one electrolyte and boost the voltage in situ to enable spontaneous yet cost-effective CO2RR. This new approach not only allows the storage of energy for overcoming the high thermodynamic barriers for the uphill CO₂RR but also allows to manufacture reactors with compact and scalable configurations, which is significant for applications that require large-volume operations such as CO₂ refinery and wastewater treatment. The MPEC bioanode prefers to operate in a neutral environment, which is the ideal condition for CO₂RR. This resolves the challenge of low water-oxidation efficiency





under neutral conditions. Furthermore, for a microbial anode, where a series of mild microbial reactions occur using self-repairing and renewal bacteria as catalysts, it was rarely confronted with stability issues, which is a major problem for semiconductor photoanodes. Whereas previous PEC systems can operate for several hours, the MPEC system in this study can operate for 29 h with photocurrent generation of 0.5–1.1 mA cm $^{-2}$, which is among the most durable systems in nonexternal-biased CO $_2$ conversion (Table S2). Lastly, the fundamental materials here are carbon brush or felt, Si, Ni, and wastewater, which are cost effective for practical applications compared with other multijunction photovoltaic systems or PEC systems which employ IrO $_2$ /RuO $_2$ as catalysts. 4,37

Syngas can also be produced by electrochemical (EC) reduction of CO_2 , where all electrons derived from water are induced by an external bias and the current density will increase with the increased bias input. Although most EC studies report higher CO_2RR current than PEC-based methods, their practical energy requirement for overall reaction will also be more than 2 V. Considering that more than 80% of electricity generated in the US is produced from nonrenewable fuels, turrent EC CO_2RR is unsustainable unless renewable electrical energy such as solar electricity is exploited. To alleviate the dependence on electricity, semiconductor-based PEC or MPEC systems directly convert solar energy and even waste chemical energy for CO_2RR with the ultimate goal to achieve a zero-external-bias system.

Syngas was the primary product of CO₂ reduction in this study due to the value and versatility that syngas brings to the chemical industry. Syngas-based organic chemical synthesis has emerged to generate liquid fuels with more carbon numbers than that of through direct CO₂ reduction. As a gaseous feedstock, CO also demonstrated higher mass transfer than H₂ gaseous feedstock.³⁹ Conventional syngas production has relied on pyrolysis and gasification of fossil fuels and is energy-intensive, while the efficient solar CO₂ conversion for syngas here addressed several issues for both energy and environmental applications. Moreover, by controlling the cathode potential (Figure 2J), the PEC method provides an easy way to tailor the products composition (CO:H₂) (Figure 5), which has been shown to greatly affect the products of syngas fermentation.⁴⁰ Among the current two routes for syngas to liquid-fuel conversion, syngas fermentation via the Wood-Ljungdahl pathway is attractive due to its lower cost, temperature and pressure conditions, and higher product selectivity compared with abiotic metal-based catalysis known as Fischer-Tropsch process.¹⁰ During a fed-batch cycle (45 h), the self-sustaining MPEC system described here generated syngas with a stoichiometric ratio (CO:H₂) at 0.6-2.3, which falls in the range of optimal ratios for gas-to-liquid-fuel conversion by fermentation.9,41

The current wastewater-treatment industry, based on fossil-fuel energy and biological degradation without energy recovery, leads to $\sim\!3\%$ of global electricity consumption and $\sim\!1.6\%$ of greenhouse-gas emissions. 42 Seeking a paradigm shift to reduce energy consumption and close the carbon loop is urgent. This work provides an alternative pathway that is capable of simultaneous CO_2 valorization and wastewater treatment. Although this proof-of-concept MPEC system demonstrated an energetically favorable way to tackle water, energy, and carbon challenges using a synergistic approach, further improvements can be done to scale the process to an engineering level. This can be realized by enhancing current density up to 30–40 mA cm $^{-2}$ via the adjustment of PMC parameters and reaction II by semiconductor and catalyst optimization. In addition, the stability of photocathodes and membranes for the prolonged operation of MPEC on a larger scale





need to be improved. A cation-exchange membrane (CEM) was used here to prevent CO diffusion between electrode compartments. Although no obvious membrane buildup of pH gradient or membrane biofouling was detected in this study, further investigation on membrane biotic and abiotic behaviors will be needed. Beyond CO₂RR, the PEC reactions occurred on the photocathode of MPEC can also be used to remove specific contaminants from wastewater, such as nitrate⁴³ and persistent organic pollutants (POPs),⁴⁴ expanding the benefits in both energy and environmental applications.

EXPERIMENTAL PROCEDURES

Resource Availability

Lead Contact

Further information and requests for resources and materials should be directed to and will be fulfilled by the Lead Contact, Jing Gu (jqu@sdsu.edu).

Materials Availability

All chemicals used in this work meet reagent grade standards of analytical purity. All chemicals were purchased from commercial resources and used as received. Singleatom Ni was supported onto nitrogen-doped carbon derived from pyrolysis of zeolitic imidazolate fromwwork-8 (ZIF-8), similar to previous literature.²⁵

Data and Code Availability

This study did not generate/analyze [datasets/code].

Chemicals, preparation procedures of Ni SA/N-C, silicon nanowires and photoelectrode, and characterization details could be found in Supplemental Information.

Microbial Photoelectrochemical (MPEC) System Construction and Operation

The cubic MPEC reactor with cylindrical chambers (5 cm in diameter) was made of acrylic plastic (Figure S10A). Two bioanodes were placed in one anode chamber (5 cm diameter × 6.2 cm length, liquid volume of 120 mL), which was separated from the cathode chamber (5 cm diameter x 3.1 cm length, liquid volume of 60 mL) containing a Si NW photocathode by a CEM (CMI-7000, Membrane International Inc., USA). Carbon fiber brushes (2.5 cm diameter \times 2.5 cm length, 0.22 m² surface area) were inoculated with the effluent obtained from a previously operating MPEC to serve as bioanodes with growth of electroactive bacteria. 16 The air cathode is made of carbon cloth (projected area 19.6 cm², 30% wet proofing, Fuel Cell Earth, Woburn, USA) with a diffusion layer and a catalyst layer (0.5 mg Pt/cm² in Vulcan XC-72 carbon black), which was used to conduct the oxygen reduction. ⁴⁵ An acrylic plastic plate with a quartz glass window was mounted at the end side of cathode chamber to allow the solar light to reach the photocathode. Ag/AgCl reference electrodes were inserted into each electrode chamber for potential measurements. The catholyte for CO_2 reduction was 0.25 M KHCO₃, and the anolyte was brewery wastewater (BWW)¹⁶ that was prepared by diluting a raw brewery wastewater collected from a local brewery by 0.2 M phosphate buffer solution (34.56 g L⁻¹ Na₂HPO₄•7H₂O, $9.80 \text{ g L}^{-1} \text{ NaH}_2\text{PO}_4 \cdot \text{H}_2\text{O}, 0.31 \text{ g L}^{-1} \text{ NH}_4\text{Cl}, 0.13 \text{ g L}^{-1} \text{ KCl})^{46}$ to a final chemical oxygen demand (COD) of 1616 \pm 70 mg L $^{-1}$. A gas-impermeable tube was connected to the bottom of the cathode chamber to allow CO2 to be sparged into the catholyte at 10 standard cubic centimeter per minute (sccm). The residual CO₂ served as carrier gas to remove the gas products (H2 and CO) away from the reactor though a port on the top of cathode chamber. The MPEC was operated in fed-batch mode, that is, the brewery wastewater (anolyte) containing waste organics was fed





into the anodic chamber for reaction until the most of biodegradable organics (electron donors) were consumed. The anolyte was then replaced with fresh wastewater.

PMC construction and PEC measurements of the MPEC system are also provided in the Supplemental Information.

SUPPLEMENTAL INFORMATION

Supplemental Information can be found online at https://doi.org/10.1016/j.joule. 2020.08.014.

ACKNOWLEDGMENTS

J.G. gratefully acknowledges Ich C. Tran at the UC Irvine Materials Research Institute for assisting with the XPS measurements and Margret Patrick to help us proofread the manuscript. The XPS work was performed at the UC Irvine Materials Research Institute (IMRI) using instrumentation funded in part by the National Science Foundation Major Research Instrumentation Program under grant no. CHE-1338173. J.G. also want to acknowledge SDSU startup funds, the SDSU University Grants Program, and NSF award CBET-1704992 to support this research. L.L. and Z.J.R. thank the support from NSF under award CBET-1834724 and support from the Andlinger Center Innovation Grant. L.L. also acknowledges the support from Shenzhen Science and Technology Program KQTD20190929172630447.

AUTHOR CONTRIBUTIONS

L.L., Z.L., J.G., and Z.J.R. wrote the manuscript. L.L., J.G., and Z.J.R. conceived the experiments. Z.L. and J.G. conducted the nanowire Si interface and single-atom Ni synthesis and characterization. L.L., X.C., and H.W. designed and adjusted the circuit. S.D. and X.P conducted the STEM and EDX measurements.

DECLARATION OF INTERESTS

The authors declare no competing interests.

Received: April 2, 2020 Revised: May 5, 2020 Accepted: August 19, 2020 Published: September 21, 2020

REFERENCES

- De Luna, P., Hahn, C., Higgins, D., Jaffer, S.A., Jaramillo, T.F., and Sargent, E.H. (2019). What would it take for renewably powered electrosynthesis to displace petrochemical processes? Science 364, eaav3506.
- Singh, M.R., Clark, E.L., and Bell, A.T. (2015). Thermodynamic and achievable efficiencies for solar-driven electrochemical reduction of carbon dioxide to transportation fuels. Proc. Natl. Acad. Sci. USA 112, E6111–E6118.
- Liu, C., Colón, B.C., Ziesack, M., Silver, P.A., and Nocera, D.G. (2016). Water splitting– biosynthetic system with CO₂ reduction efficiencies exceeding photosynthesis. Science 352. 1210–1213.
- Schreier, M., Curvat, L., Giordano, F., Steier, L., Abate, A., Zakeeruddin, S.M., Luo, J., Mayer, M.T., and Grätzel, M. (2015). Efficient photosynthesis of carbon monoxide from CO₂

- using perovskite photovoltaics. Nat. Commun. 6, 7326.
- White, J.L., Baruch, M.F., Pander Iii, J.E., III, Hu, Y., Fortmeyer, I.C., Park, J.E., Zhang, T., Liao, K., Gu, J., Yan, Y., et al. (2015). Light-driven heterogeneous reduction of carbon dioxide: photocatalysts and photoelectrodes. Chem. Rev. 115, 12888–12935.
- Zhang, N., Long, R., Gao, C., and Xiong, Y. (2018). Recent progress on advanced design for photoelectrochemical reduction of CO₂ to fuels. Sci. China Mater. 61, 771–805.
- Andrei, V., Reuillard, B., and Reisner, E. (2020). Bias-free solar syngas production by integrating a molecular cobalt catalyst with perovskite–BiVO₄ tandems. Nat. Mater. 19, 189–194.

- Jang, Y.J., Jeong, I., Lee, J., Lee, J., Ko, M.J., and Lee, J.S. (2016). Unbiased sunlight-driven artificial photosynthesis of carbon monoxide from CO₂ using a ZnTe-based photocathode and a perovskite solar cell in tandem. ACS Nano 10, 6980–6987.
- Sun, X., Atiyeh, H.K., Huhnke, R.L., and Tanner, R.S. (2019). Syngas fermentation process development for production of biofuels and chemicals: a review. Bioresour. Technol. Rep. 7, 100279.
- Khodakov, A.Y., Chu, W., and Fongarland, P. (2007). Advances in the development of novel cobalt Fischer-Tropsch catalysts for synthesis of long-chain hydrocarbons and clean fuels. Chem. Rev. 107, 1692–1744.
- 11. Logan, B.E., and Rabaey, K. (2012). Conversion of wastes into bioelectricity and chemicals by

Joule Article



- using microbial electrochemical technologies. Science 337, 686–690.
- Lu, L., Lobo, F.L., Xing, D., and Ren, Z.J. (2019). Active harvesting enhances energy recovery and function of electroactive microbiomes in microbial fuel cells. Appl. Energy 247, 492–502.
- Qian, F., Wang, G., and Li, Y. (2010). Solardriven microbial photoelectrochemical cells with a nanowire photocathode. Nano Lett. 10, 4686–4691.
- Lu, L., Williams, N.B., Turner, J.A., Maness, P.C., Gu, J., and Ren, Z.J. (2017). Microbial photoelectrosynthesis for self-sustaining hydrogen generation. Environ. Sci. Technol. 51, 13494–13501.
- 15. Zang, G.-L., Sheng, G.-P., Shi, C., Wang, Y.-K., Li, W.-W., and Yu, H.-Q. (2014). A biophotoelectrochemical cell with a MoS₃modified silicon nanowire photocathode for hydrogen and electricity production. Energy Environ. Sci. 7, 3033–3039.
- 16. Lu, L., Vakki, W., Aguiar, J.A., Xiao, C., Hurst, K., Fairchild, M., Chen, X., Yang, F., Gu, J., and Ren, Z.J. (2019). Unbiased solar H₂ production with current density up to 23 mA cm⁻² by Swisscheese black Si coupled with wastewater bioanode. Energy Environ. Sci. 12, 1088–1099.
- Lu, L., and Ren, Z.J. (2016). Microbial electrolysis cells for waste biorefinery: a state of the art review. Bioresour. Technol. 215, 254–264.
- Suraniti, E., Merzeau, P., Roche, J., Gounel, S., Mark, A.G., Fischer, P., Mano, N., and Kuhn, A. (2018). Uphill production of dihydrogen by enzymatic oxidation of glucose without an external energy source. Nat. Commun. 9, 3229.
- Schneider, J., and Bahnemann, D.W. (2013). Undesired role of sacrificial reagents in photocatalysis. J. Phys. Chem. Lett. 4, 3479– 3483
- Heidrich, E.S., Edwards, S.R., Dolfing, J., Cotterill, S.E., and Curtis, T.P. (2014).
 Performance of a pilot scale microbial electrolysis cell fed on domestic wastewater at ambient temperatures for a 12month period. Bioresour. Technol. 173, 87–95.
- Chen, X., Lobo, F.L., Bian, Y., Lu, L., Chen, X., Tucker, M.P., Wang, Y., and Ren, Z.J. (2020). Electrical decoupling of microbial electrochemical reactions enables spontaneous H₂ evolution. Energy Environ. Sci. 13, 495–502.
- Liu, R., Yuan, G., Joe, C.L., Lightburn, T.E., Tan, K.L., and Wang, D. (2012). Silicon nanowires as photoelectrodes for carbon dioxide fixation. Angew. Chem. Int. Ed. 51, 6709–6712.

- Yang, H.B., Hung, S.-F., Liu, S., Yuan, K., Miao, S., Zhang, L., Huang, X., Wang, H.-Y., Cai, W., Chen, R., et al. (2018). Atomically dispersed Ni (I) as the active site for electrochemical CO₂ reduction. Nat. Energy 3, 140–147.
- Zheng, T., Jiang, K., Ta, N., Hu, Y., Zeng, J., Liu, J., and Wang, H. (2019). Large-scale and highly selective CO₂ electrocatalytic reduction on nickel single-atom catalyst. Joule 3, 265–278.
- Zhao, C., Dai, X., Yao, T., Chen, W., Wang, X., Wang, J., Yang, J., Wei, S., Wu, Y., and Li, Y. (2017). Ionic exchange of metal–organic frameworks to access single nickel sites for efficient electroreduction of CO₂. J. Am. Chem. Soc. 139, 8078–8081.
- Crewe, A.V., Wall, J., and Langmore, J. (1970). Visibility of single atoms. Science 168, 1338– 1340.
- Kabir, S., Artyushkova, K., Serov, A., Kiefer, B., and Atanassov, P. (2016). Binding energy shifts for nitrogen-containing graphene-based electrocatalysts- experiments and DFT calculations. Surf. Interface Anal. 48, 293–300.
- 28. Zhang, C., Sha, J., Fei, H., Liu, M., Yazdi, S., Zhang, J., Zhong, Q., Zou, X., Zhao, N., Yu, H., et al. (2017). Single-atomic ruthenium catalytic sites on nitrogen-doped graphene for oxygen reduction reaction in acidic medium. ACS Nano 11, 6930–6941.
- Jiang, K., Siahrostami, S., Zheng, T., Hu, Y., Hwang, S., Stavitski, E., Peng, Y., Dynes, J., Gangisetty, M., Su, D., et al. (2018). Isolated Ni single atoms in graphene nanosheets for highperformance CO₂ reduction. Energy Environ. Sci. 11, 893–903.
- Jia, M., Choi, C., Wu, T.S., Ma, C., Kang, P., Tao, H., Fan, Q., Hong, S., Liu, S., Soo, Y.-L., et al. (2018). Carbon-supported Ni nanoparticles for efficient CO₂ electroreduction. Chem. Sci. 9, 8775–8780.
- Sun, Z., Ma, T., Tao, H., Fan, Q., and Han, B. (2017). Fundamentals and challenges of electrochemical CO₂ reduction using twodimensional materials. Chem 3, 560–587.
- Ren, W., Tan, X., Yang, W., Jia, C., Xu, S., Wang, K., Smith, S.C., and Zhao, C. (2019). Isolated diatomic Ni-Fe metal-nitrogen sites for synergistic electroreduction of CO₂. Angew. Chem. Int. Ed. 58, 6972–6976.
- Walter, M.G., Warren, E.L., McKone, J.R., Boettcher, S.W., Mi, Q., Santori, E.A., and Lewis, N.S. (2010). Solar water splitting cells. Chem. Rev. 110, 6446–6473.
- Yang, Y., Wang, M., Zhang, P., Wang, W., Han, H., and Sun, L. (2016). Evident enhancement of photoelectrochemical hydrogen production by electroless deposition of M-B (M = Ni, Co)

- catalysts on silicon nanowire arrays. ACS Appl. Mater. Interfaces *8*, 30143–30151.
- Waugh, K.C. (1992). Methanol synthesis. Catal. Today 15, 51–75.
- Peng, X.D., Wang, A.W., Toseland, B.A., and Tijm, P.J.A. (1999). Single-step syngas-todimethyl ether processes for optimal productivity, minimal emissions, and natural gas-derived syngas. Ind. Eng. Chem. Res. 38, 4381–4388.
- Arai, T., Sato, S., and Morikawa, T. (2015). A monolithic device for CO₂ photoreduction to generate liquid organic substances in a singlecompartment reactor. Energy Environ. Sci. 8, 1998–2002.
- 38. U.S. Energy Information Administration (2019). Electricity in the United States. https://www.eia.gov/energyexplained/electricity/electricity-in-the-us.php.
- Munasinghe, P.C., and Khanal, S.K. (2014). Evaluation of hydrogen and carbon monoxide mass transfer and a correlation between the myoglobin-protein bioassay and gas chromatography method for carbon monoxide determination. RSC Adv. 4, 37575–37581.
- Jack, J., Lo, J., Maness, P.-C., and Ren, Z.J. (2019). Directing Clostridium ljungdahlii fermentation products via hydrogen to carbon monoxide ratio in syngas. Biomass Bioenergy 124, 95–101.
- Phillips, J.R., Huhnke, R.L., and Atiyeh, H.K. (2017). Syngas fermentation: a microbial conversion process of gaseous substrates to various products. Fermentation 3, 28.
- Lu, L., Guest, J.S., Peters, C.A., Zhu, X., Rau, G.H., and Ren, Z.J. (2018). Wastewater treatment for carbon capture and utilization. Nat Sustain. 1, 750–758.
- Wang, H., and Turner, J.A. (2015). Photoelectrochemical reduction of nitrates at the illuminated p-GalnP₂ photoelectrode. Energy Environ. Sci. 8, 1046.
- Li, F., Duan, J., Tian, S., Ji, H., Zhu, Y., Wei, Z., and Zhao, D. (2020). Short-chain per-and polyfluoroalkyl substances in aquatic systems: occurrence, impacts and treatment. Chem. Eng. J. 380, 122506.
- Lu, L., Huang, Z., Rau, G.H., and Ren, Z.J. (2015). Microbial electrolytic carbon capture for carbon negative and energy positive wastewater treatment. Environ. Sci. Technol. 49, 8193–8201.
- Lu, L., Hou, D., Fang, Y., Huang, Y., and Ren, Z.J. (2016). Nickel based catalysts for highly efficient H₂ evolution from wastewater in microbial electrolysis cells. Electrochim. Acta 206, 381–387.